

Determining the equation of state of neutron stars with Einstein Telescope using tidal effects and r-mode excitations from a population of binary inspirals

Pawan Kumar Gupta^{1,2}, Anna Puecher^{1,2}, Peter T.H. Pang^{1,2},
Justin Janquart^{1,2}, Gideon Koekoek^{1,3}, and Chris Van Den Broeck^{1,2}
¹*Nikhef – National Institute for Subatomic Physics,
Science Park 105, 1098 XG Amsterdam, The Netherlands*
²*Institute for Gravitational and Subatomic Physics (GRASP),
Utrecht University, Princetonplein 1, 3584 CC Utrecht, The Netherlands and*
³*Department of Gravitational Waves and Fundamental Physics,
Maastricht University, P.O. Box 616, 6200 MD Maastricht, The Netherlands*
(Dated: May 4, 2022)

Third-generation gravitational wave (GW) observatories such as Einstein Telescope (ET) and Cosmic Explorer (CE) will be ideal instruments to probe the structure of neutron stars through the GWs they emit when undergoing binary coalescence. In this work we make predictions about how well ET in particular will enable us to reconstruct the neutron star equation of state through observations of tens of binary neutron star coalescences with signal-to-noise ratios in the hundreds. We restrict ourselves to information that can be extracted from the inspiral, which includes tidal effects and possibly r-mode resonances. In treating the latter we go beyond the Newtonian approximation, introducing and utilizing new universal relations. We find that the ability to observe resonant r-modes would have a noticeable impact on neutron star equation of state measurements with ET.

I. INTRODUCTION

The detection with Advanced LIGO [1] and Advanced Virgo [2] of gravitational waves (GWs) from the binary neutron star (BNS) coalescences GW170817 [3] and GW190425 [4], together with electromagnetic observations [5–7] has already had a significant impact on our insight into the structure of neutron stars; for a recent review, see e.g. [8]. Even so, the neutron star equation of state (EOS) remains poorly constrained. This is expected to change with the advent of third-generation GW detectors such as Einstein Telescope (ET) [9, 10] and Cosmic Explorer (CE) [11, 12], which are likely to see hundreds of thousands of binary neutron star coalescences, of which hundreds may have signal-to-noise ratios (SNRs) in excess of 100; see [13] for recent estimates. Whereas with current detectors we only have access to the inspiral signal, ET and CE will also probe the post-merger [14, 15].

In this paper we will quantify to what extent the equation of state – essentially pressure versus density, $p(\rho)$ – of neutron stars can be probed with third-generation GW observatories, based on inspiral physics alone. The main EOS-related effect that enters the inspiral signal is that of tides on the neutron stars [16, 17]. These can already be investigated with second-generation detectors [18–20], as has indeed been done with GW170817 [3, 21, 22]. Tidal effects are the most noticeable at high frequencies. However, given sufficiently high SNR, it may also be possible to see resonant r-modes [23], gravitomagnetic excitations of Rossby modes that are induced when the monotonically increasing GW frequency reaches an associated resonance frequency of one of the neutron stars. Assuming slowly rotating neutron stars, these will mainly manifest themselves at lower frequen-

cies, i.e. tens of Hz. Though the imprints of resonant r-modes on GW signals will generally be weak, they can be within reach of third-generation observatories [24]. Moreover, as recently indicated by Ma et al. [25], EOS measurements may gain from the ability to access r-mode information in addition to tidal effects. In this study we will focus on ET, in part because it is predicted to have excellent low frequency sensitivity.

In [25], Fisher matrix estimates were made to assess the measurability of tidal deformabilities and other parameters related to neutron stars in binary inspiral, with or without resonant r-modes. For the purpose of initial estimates, in the latter paper the r-modes were largely treated in the Newtonian approximation, but it is known that relativistic corrections on both the resonance frequency and the size of the induced GW phase shift can be sizeable; see e.g. [26–28]. Here we do take such corrections into account, and we introduce and use new universal relations for both. Moreover, we want to know what is the impact of having a sizeable number of high-SNR BNS signals at one’s disposal. Ideally we would want to perform Bayesian parameter estimation simulations, but limited computational resources prevent us from doing so. As a compromise, we will still use the Fisher matrix to obtain multivariate Gaussian approximations for the likelihoods of individual sources, but we sample from those to obtain estimates for EOS measurements with input from multiple detected sources. Recently, catalogs of binary black hole and binary neutron star detections by ET and CE were simulated [13] based on predictions for merger rate as a function of redshift; we will draw from this work to obtain a representative sample for the 20 loudest BNS signals that ET is likely to detect based on its predicted sensitivity curve. Based on these we will arrive at esti-

mates for how accurately one will be able to reconstruct $p(\rho)$ with observations by ET, with or without r-modes.

The rest of this paper is structured as follows. In Sec. II we describe our treatment of resonant r-modes in terms of universal relations. In Sec. III we explain the setup of our analyses. Results are given in Sec. IV. Finally, an overview and conclusions are presented in Sec. V. Unless stated otherwise, throughout this paper we set $G = c = 1$.

II. RESONANT R-MODES: FREQUENCIES, PHASE SHIFTS, AND UNIVERSAL RELATIONS

As two neutron stars spiral towards each other, the GW frequency increases monotonically, and at one or more points in time it can become equal to an internal resonance frequency of one of the neutron stars. The resulting excitation takes away part of the orbital energy, which speeds up the orbital motion; this in turn gets imprinted upon the phasing of the GW signal. Assuming the two neutron star each undergo near-instantaneous resonances at respective frequencies $f_0^{(1,2)}$, the resulting change in the frequency-domain GW phase with respect to the point particle case can be modeled as [16, 23]

$$\Psi_r = \left(1 - \frac{f}{f_0^{(1)}}\right) \Delta\Phi_1 \Theta(f - f_0^{(1)}) + \left(1 - \frac{f}{f_0^{(2)}}\right) \Delta\Phi_2 \Theta(f - f_0^{(2)}), \quad (1)$$

where $\Theta(x)$ denotes the usual step function. Specializing to r-mode excitations, the shifts $\Delta\Phi_i$, $i = 1, 2$ take the form [25]

$$\Delta\Phi_i = -2 \frac{5\pi^2}{192} \left(\frac{4}{3}\right)^{2/3} \frac{\Omega_i^{2/3}}{\mathcal{M}^{10/3}} \mathcal{I}_i. \quad (2)$$

Here Ω_i , $i = 1, 2$ are the angular rotation frequencies of the neutron stars, and $\mathcal{M} = (m_1 m_2)^{3/5} / (m_1 + m_2)^{1/5}$ is the chirp mass associated with the component masses m_1, m_2 . The r-mode couplings \mathcal{I}_i take the form

$$\mathcal{I}_i = (\bar{I}_i^r)^2 m_i^4 \sin^2(\psi_i) \cos^4(\psi_i/2) \left(1 - \frac{m_i}{M}\right), \quad (3)$$

where $M = m_1 + m_2$ is the total mass, and ψ_i are the angles between the neutron stars' spin vectors \mathbf{S}_i and the orbital angular momentum. The r-mode *overlaps* \bar{I}_i^r depend on the neutron stars' internal structure.

Let us now discuss in turn our treatment of r-mode frequencies and overlaps.

A. Universal relation for the r-mode frequencies

For a slowly rotating neutron stars and in the Newtonian limit, the r-mode frequencies in the co-rotating

frame are proportional to the angular rotation frequency Ω , and given by [23]

$$\omega_{\ell m} = -\frac{2m}{\ell(\ell+1)}\Omega. \quad (4)$$

For given values of the spherical harmonic indices (ℓ, m) , the corresponding resonance frequency in the inertial frame is

$$\omega_0 = m\Omega + \omega_{\ell m} = m\Omega - \frac{2m}{\ell(\ell+1)}\Omega. \quad (5)$$

The associated GW frequencies appearing in Eq. (1) are then $f_0 = 2\omega_0/(2\pi)$, or

$$f_0 = \frac{1}{\pi}(m - \kappa)\Omega, \quad (6)$$

with $\kappa = 2m/\ell(\ell+1)$ in the Newtonian limit. For simplicity, in this work we will assume barotropic neutron stars, so that $|m| = \ell$, and focus on $(\ell, m) = (2, 2)$; within the Newtonian framework one then has $\kappa = 2/3$.

As shown in [26], in a relativistic treatment of slowly rotating stars, the resonance frequency can differ significantly from the Newtonian value. In that work, numerical values for κ were computed for relativistic neutron stars described by a variety of tabulated EOSs, and a fitting formula was obtained for the function $\kappa(C)$, with $C = m/R$ the compactness, where R is a neutron star's radius. However, in this work we are interested in the imprint of resonant r-modes on GW emission, where it is more convenient to have κ as function of the dimensionless neutron star tidal deformability Λ , since this is a parameter that enters directly into the waveform.

With this in mind, for each value of κ reported in [26] (Table II), we computed Λ for each EOS and compactness listed. This was done using the TOV solver available in LALSuite [29]. As seen in Fig. 1, there is a clear dependence of κ on the logarithm of Λ . Using a least-squares fitting method, we find that the functional dependence is approximated well by the universal relation

$$\kappa = 0.3668 + 0.0498 \log(\Lambda) - 0.0025 \log^2(\Lambda), \quad (7)$$

with fitting residuals at the $\mathcal{O}(1\%)$ level.

B. Universal relation for the r-mode overlap

Next we turn to the r-mode overlap. In the Newtonian approximation one has [25]

$$\bar{I}^r = \sqrt{\frac{1}{m^5} \int_0^R \rho r^6 dr}, \quad (8)$$

where ρ is the density of the neutron star, m its mass, and R its radius. In [25], a universal relation was obtained for the Newtonian \bar{I}^r as function of Λ . In this

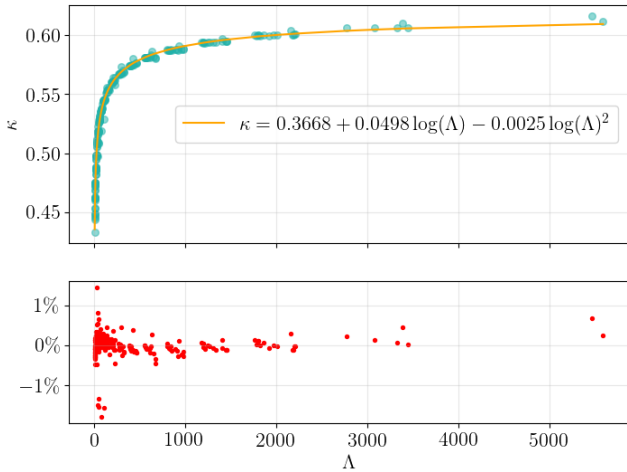


FIG. 1. Top panel: values of κ and corresponding tidal deformabilities Λ computed for a variety of EOSs and compactnesses listed in [26] (green dots), and the fit for $\kappa(\Lambda)$ of Eq. 7. Bottom panel: fitting residuals.

work we instead follow the relativistic description of [27], where the following expression was found:

$$\bar{I}^r = \sqrt{\frac{15}{4\pi}(\Sigma_{\text{stat}} - \Sigma_{\text{irr}})}. \quad (9)$$

Here Σ_{stat} and Σ_{irr} are dimensionless static and irrotational magnetic Love numbers, respectively. Universal relations for these quantities as function of Λ were derived in [28], which for completeness we display again here:

$$\begin{aligned} \log(-\Sigma_{\text{irr}}) &= -2.03 + 0.487 \log(\Lambda) + 9.69 \times 10^{-3} \log^2(\Lambda) \\ &\quad + 1.03 \times 10^{-3} \log^3(\Lambda) - 9.37 \times 10^{-5} \log^4(\Lambda) \\ &\quad + 2.24 \times 10^{-6} \log^5(\Lambda), \end{aligned} \quad (10)$$

$$\begin{aligned} \log(\Sigma_{\text{stat}}) &= -2.66 + 0.786 \log(\Lambda) - 1.00 \times 10^{-2} \log^2(\Lambda) \\ &\quad + 1.28 \times 10^{-3} \log^3(\Lambda) - 6.37 \times 10^{-5} \log^4(\Lambda) \\ &\quad + 1.18 \times 10^{-6} \log^5(\Lambda). \end{aligned} \quad (11)$$

Together with Eq. (9), these yield a relation for $\bar{I}^r(\Lambda)$.

III. SETUP OF THE ANALYSES

In this section we describe the waveform model used, the Fisher matrix formalism for obtaining a multivariate Gaussian approximation of likelihoods, the parameterization used for reconstructing EOSs, and our framework for performing such reconstructions using multiple GW detections.

A. Waveform model

We will focus on the inspiral, and use an analytic, frequency domain waveform following the stationary phase approximation [30], which takes the general form

$$\tilde{h}(f) = \mathcal{A} f^{-7/6} e^{i\Psi(f)}. \quad (12)$$

Here \mathcal{A} collects parameters appearing in the amplitude: masses, sky position, orientation of the orbital plane, and luminosity distance to the source. The phase $\Psi(f)$ can be written as

$$\Psi(f) = \Psi_{\text{PP}}(f) + \Psi_{\text{SO}}(f) + \Psi_{\text{T}}(f) + \Psi_r(f), \quad (13)$$

where Ψ_{PP} has point particle contributions up to 3.5 post-Newtonian (PN) order, and Ψ_{SO} contains spin-orbit effects at 1.5PN; we consider spin-spin effects to be negligible in the case of binary neutron stars. (For a review of the post-Newtonian approximation, see [31].) Ψ_{T} contains tidal effects at 5PN and 6PN orders [32]. Finally, Ψ_r is as given in Eq. (1), and we note that to good approximation, the angles $\psi_{1,2}$ entering Eq. (3) can usually be considered approximately constant even in the presence of spin precession [33–35].

Without the r-mode contribution, the phase depends on the 8 free parameters

$$\vec{\theta}_{nr} = (t_c, \phi_c, m_1, m_2, \tilde{\Lambda}, \delta\tilde{\Lambda}, \chi_{sz}, \chi_{az}), \quad (14)$$

whereas with r-modes included, the free parameters are

$$\vec{\theta}_r = (t_c, \phi_c, m_1, m_2, \tilde{\Lambda}, \delta\tilde{\Lambda}, \Omega_1, \Omega_2, \psi_1, \psi_2). \quad (15)$$

Here t_c and ϕ_c are respectively the time and phase of coalescence; m_i , $i = 1, 2$ the component masses; $\chi_{sz} = (\chi_{1z} + \chi_{2z})/2$ and $\chi_{az} = (\chi_{1z} - \chi_{2z})/2$ respectively the symmetric and antisymmetric dimensionless spins, with χ_{1z} and χ_{2z} the spin components in the direction of orbital angular momentum; Ω_i the spin angular frequencies of the neutron stars; and ψ_i the angles between the dimensionless spins and the orbital angular momentum. We note that in the detector frame, the component masses $m_{1,2}^{\text{det}}$ that directly enter the waveform are redshifted with respect to the source frame masses $m_{1,2}$: one has $m_{1,2}^{\text{det}} = (1+z)m_{1,2}$, with z the redshift. With a global network of third-generation (3G) observatories, for BNS signals the luminosity distance can be measured to $\mathcal{O}(1\%)$ accuracy for the loudest sources [36], and with a cosmological model (e.g. from Planck [37]), distance can be converted to redshift. We will assume that other 3G observatories will be operational at the same time as ET, so that for the high-SNR sources considered below, the distance uncertainties will be sufficiently small that uncertainties on redshift can be neglected in the conversion between source frame and detector frame masses. Finally, $\tilde{\Lambda}$ and $\delta\tilde{\Lambda}$ are related to the individual neutron stars' tidal deformability param-

eters (Λ_1, Λ_2) through [38]

$$\tilde{\Lambda} = \frac{8}{3} \left[(1 + 7\eta - 31\eta^2)(\Lambda_1 + \Lambda_2) + \sqrt{1 - 4\eta}(1 + 9\eta - 11\eta^2)(\Lambda_1 - \Lambda_2) \right], \quad (16)$$

$$\delta\tilde{\Lambda} = \frac{1}{2} \left[\sqrt{1 - 4\eta} \left(1 - \frac{13272}{1319}\eta + \frac{8944}{1319}\eta^2 \right) (\Lambda_1 + \Lambda_2) + \left(1 - \frac{15910}{1319}\eta + \frac{32850}{1319}\eta^2 + \frac{3380}{1319}\eta^3 \right) (\Lambda_1 - \Lambda_2) \right], \quad (17)$$

where $\eta = m_1 m_2 / (m_1 + m_2)^2$ is the symmetric mass ratio.

When comparing the cases with and without r-modes, we can use that

$$\chi_{iz} = \bar{I}_i \Omega_i m_i \cos(\psi_i) \quad (18)$$

for $i = 1, 2$. Here \bar{I}_i are normalized moments of inertia, for which one has the universal relation [39]

$$\log \bar{I} = 1.47 + 8.17 \times 10^{-2} \log(\Lambda) + 1.49 \times 10^{-2} \log^2(\Lambda) + 2.87 \times 10^{-4} \log^3(\Lambda) - 3.64 \times 10^{-5} \log^4(\Lambda). \quad (19)$$

B. Spectral parametrization of the EOS

For the EOS we will use the so-called spectral parametrization in terms of the adiabatic index $\Gamma(p)$, defined as [40, 41]

$$\Gamma(p) = \frac{\epsilon + p}{p} \frac{dp}{d\epsilon}, \quad (20)$$

where ϵ is energy density and p is pressure. The EOS $\epsilon(p)$ is obtained from the adiabatic index by writing the above equation as

$$\frac{d\epsilon}{dp} = \frac{\epsilon(p) + p}{p\Gamma(p)}, \quad (21)$$

or

$$\epsilon(p) = \frac{\epsilon_0}{\mu(p)} + \frac{1}{\mu(p)} \int_{p_0}^p \frac{\mu(p')}{\Gamma(p')} dp', \quad (22)$$

where

$$\mu(p) = \exp \left(- \int_{p_0}^p \frac{1}{p'\Gamma(p')} dp' \right), \quad (23)$$

with $\epsilon_0 = \epsilon(p_0)$ a constant of integration. The EOS $\epsilon(p)$ can in principle be solved for arbitrary adiabatic index $\Gamma(p)$, but here we will spectrally decompose it in terms of a set of polynomial basis functions,

$$\Gamma(p) = \exp \left(\sum_{k=0}^n \gamma_k x^k \right), \quad (24)$$

where $x = \log(p/p_0)$ is a dimensionless pressure variable, p_0 is some reference pressure, and values of n up to 3 tend to allow for accurate representations of a variety of EOSs [41].

For given coefficients γ_k in Eq. (24), the TOV solver available in LALSuite [29] numerically performs the integrals in Eqs. (23) and (22) to obtain $\epsilon(p)$ and rest mass density $\rho(p)$, which is inverted to arrive at $p(\rho)$. The reference pressure p_0 , also called the stitching pressure, is fixed to 5.3716×10^{32} dyne cm^{-2} ; below this pressure, the EOS called SLY [42] is stitched on. The coefficients γ_k , $k = 0, \dots, 3$ are given uniform priors with ranges $\gamma_0 \in [0.2, 2.0]$, $\gamma_1 \in [-1.6, 1.7]$, $\gamma_2 \in [-0.6, 0.6]$, and $\gamma_3 \in [-0.02, 0.02]$. The speed of sound $v_s = \sqrt{dp/d\epsilon}$ is restricted to $v_s < 1.1c$, where the 10% leeway is to allow for imperfect parameterization. Finally, the adiabatic index is confined to $\Gamma(p) \in [0.6, 4.5]$ [21].

C. Analysis framework

Let θ^a be the components of the parameter vector $\vec{\theta}$, which in our case will be either the one from Eq. (14) or (15), depending on whether or not r-modes are taken into account. For GW events with sufficiently high SNR and assuming stationary, Gaussian noise, the likelihood function for the signal parameters θ^a will approximately take the form of a multivariate Gaussian centered on the true values θ^a [43, 44]. Defining $\Delta\theta^a = \theta^a - \theta^a$, the likelihood becomes

$$L(\Delta\theta^a) = \mathcal{N} e^{-\frac{1}{2} \Gamma_{ab} \Delta\theta^a \Delta\theta^b}, \quad (25)$$

where \mathcal{N} is a normalization factor, and sums over a and b are implied. The *Fisher matrix* is given by

$$\Gamma_{ab} = \left\langle \frac{\partial h}{\partial \theta^a} \middle| \frac{\partial h}{\partial \theta^b} \right\rangle, \quad (26)$$

where the noise-weighted inner product $\langle \cdot | \cdot \rangle$ is defined as

$$\langle h | g \rangle = 4\Re \int_{f_{\text{low}}}^{f_{\text{high}}} \frac{\tilde{h}^*(f) \tilde{g}(f)}{S_n(f)} df, \quad (27)$$

with $S_n(f)$ the one-sided noise power spectral density (PSD).

Strictly speaking, Eq. (25) with (26) pertains to signals $\tilde{h}(f)$ as seen in a *single* detector, while the baseline design for Einstein Telescope assumes three V-shaped detectors arranged in a triangle [9, 10]. In principle one would then have to project the gravitational wave polarizations $\tilde{h}_+(f)$, $\tilde{h}_\times(f)$ onto each of the three detectors using the appropriate antenna pattern functions, construct a separate Fisher matrix for each detector, and take the sum of these to obtain the final Fisher matrix. In this work we will consider sources from a catalog constructed as in [13], with SNRs computed for a triangular ET. However, since here we will mainly be

interested in information coming from the phasing, for our purposes it will suffice to compute a single Fisher matrix with the ET-D PSD [10] for an L-shaped detector, and with the SNRs set to the values obtained from the triangular ET. In Eq. (27) we take the lower frequency cut-off f_{low} to be 5 Hz. For f_{high} we choose the nominal frequency of the innermost stable circular orbit (ISCO): $f_{\text{high}} = 1/(6^{3/2}\pi(1+z)M)$. We note that for stiff EOSs, the two neutron stars might touch before ISCO is reached [19], but the effect of this for the purposes of EOS measurements is marginal [38].

Since we are interested in how well one can measure the EOS with BNS inspiral signals, we need to choose a “true” EOS, which we take to be FPS [45], with $(\gamma_0, \gamma_1, \gamma_2, \gamma_3) = (1.1561, -0.0468, 0.0081, -0.0010)$. Given a choice of masses m_1, m_2 , we let the true values of the tidal deformabilities be $\Lambda_1 = \Lambda_{\text{FPS}}(m_1)$, $\Lambda_2 = \Lambda_{\text{FPS}}(m_2)$, where $\Lambda_{\text{FPS}}(m)$ is the dependence set by the given EOS.

The main question in this work is how well ET will be able to determine the EOS, i.e., with what accuracy the EOS parameters $\vec{E} \equiv (\gamma_0, \gamma_1, \gamma_2, \gamma_3)$ will be measured. To this end, consider the posterior probability density function $p(\vec{E}, \vec{\theta}'|d, \mathcal{H}, \mathcal{I})$, where $\vec{\theta}'$ denotes the parameters in (14) or (15) *except* for $\tilde{\Lambda}$ and $\delta\tilde{\Lambda}$, which can be calculated from \vec{E} together with m_1, m_2 ; other than that, d denotes the data for a given signal, \mathcal{H} a waveform model, and \mathcal{I} any background information we may possess. Bayes’ theorem tells us that

$$p(\vec{E}, \vec{\theta}'|d, \mathcal{H}, \mathcal{I}) = \frac{p(d|\vec{E}, \vec{\theta}', \mathcal{H}, \mathcal{I})p(\vec{E}, \vec{\theta}'|\mathcal{H}, \mathcal{I})}{p(d|\mathcal{H}, \mathcal{I})}, \quad (28)$$

where $p(\vec{E}, \vec{\theta}'|\mathcal{H}, \mathcal{I})$ is the prior probability density for \vec{E} and $\vec{\theta}'$, $p(d|\vec{E}, \vec{\theta}', \mathcal{H}, \mathcal{I})$ the likelihood, and $p(d|\mathcal{H}, \mathcal{I})$ the evidence, which is set by the requirement that the posterior probability density be normalized. Clearly $p(d|\vec{E}, \vec{\theta}', \mathcal{H}, \mathcal{I})$ is not quite the same as the likelihood $L(\Delta\theta^a)$ obtained from the Fisher matrix in Eq. (25), but given true values $\hat{\theta}^a$ for the parameters entering the waveform, it is possible to relate the two by writing

$$\begin{aligned} L(\Delta\theta^a) &= p(d|\vec{\theta}, \mathcal{H}, \mathcal{I}) \\ &= p(d|\{\tilde{\Lambda}_{\vec{E}}(m_1, m_2), \delta\tilde{\Lambda}_{\vec{E}}(m_1, m_2), \vec{\theta}'\}, \mathcal{H}, \mathcal{I}) \\ &= p(d|\{\vec{E}, \vec{\theta}'\}, \mathcal{H}, \mathcal{I}), \end{aligned} \quad (29)$$

where in the second line, $\tilde{\Lambda}_{\vec{E}}(m_1, m_2)$ and $\delta\tilde{\Lambda}_{\vec{E}}(m_1, m_2)$ are the $\tilde{\Lambda}$ and $\delta\tilde{\Lambda}$ obtained from the component masses for an EOS with the given parameters \vec{E} , and the likelihood in the last line is the one appearing in Eq. (28).

The way we will proceed is then as follows. Using the Fisher matrix we compute the likelihood of Eq. (25), and with the identification of Eq. (29) this is turned into a likelihood in terms of the EOS parameters \vec{E} and waveform parameters $\vec{\theta}'$. We choose flat priors for all of the individual parameters, and using the `emcee` sampler [46] we obtain the posterior density in Eq. (28).

By integrating out the $\vec{\theta}'$, this gives us a posterior density for the \vec{E} , $p(\vec{E}|d, \mathcal{H}, \mathcal{I})$.¹ So far we have focused on a single signal, but given a catalog of detected signals d_1, d_2, \dots, d_N that are considered independent,² information from all of them can be combined to obtain [18]

$$\begin{aligned} p(\vec{E}|d_1, d_2, \dots, d_N, \mathcal{H}, \mathcal{I}) \\ = p(\vec{E}|\mathcal{H}, \mathcal{I})^{1-N} \prod_{n=1}^N p(\vec{E}|d_n, \mathcal{H}, \mathcal{I}), \end{aligned} \quad (30)$$

where in practice the posteriors in the product are Gaussian kernel density estimates of the ones obtained directly with `emcee`. Through the TOV solver of LALSuite [29], the above combined posterior distribution for \vec{E} leads to a distribution over equations of state $p(\rho)$.

Sources are picked from a catalog constructed as in [13]. For binary neutron stars this assumes uniformly distributed source frame component masses, where for the primary mass $m_1 \in [1 M_\odot, M_{\text{max}}]$ and for the secondary mass $m_2 \in [1 M_\odot, m_1]$; here we take M_{max} to be the maximum mass supported by our reference EOS, which is $M_{\text{max}} = 2.03 M_\odot$. As explained in Sec. III A, we will assume that for the highest-SNR sources, distances can be measured with sufficient accuracy that uncertainties on redshift can be neglected in the conversion between source frame masses and detector frame masses. The sources were distributed over comoving distance according to a particular prediction for the merger rate as a function of redshift; for details we refer to the original paper [13]. ET is likely to see tens of thousands of BNSs per year, but it is reasonable to expect that most of the information will come from the loudest sources. Hence we consider the 20 loudest sources in the catalog, which have SNRs between 154 and 368. The angles between the spin vectors and the orbital angular momentum are taken to be uniform on the sphere. The rotation angular frequencies of the neutron stars are taken to be uniform in the intervals $\Omega_i \in [0, 2\pi \times 45]$ Hz, $i = 1, 2$ [47]. Given these ranges for the Ω_i and the assumed detector lower frequency cut-off of $f_{\text{low}} = 5$ Hz, there is a small chance for the r-mode GW frequency f_0 in Eq. (6) to be below f_{low} for one or both neutron stars in a binary, but this will not be the case for any of the simulated sources considered here. We will perform

¹ In principle we could have set $\tilde{\Lambda} = \tilde{\Lambda}_{\vec{E}}(m_1, m_2)$ and $\delta\tilde{\Lambda} = \delta\tilde{\Lambda}_{\vec{E}}(m_1, m_2)$ directly in the Fisher matrix, and obtained 1-sigma uncertainties on the components of \vec{E} from the covariance matrix in the usual way [43, 44]. However, introducing too many additional parameters can lead to ill-conditioned Fisher matrices, which will cause problems with numerical inversion.

² If all neutron stars follow the same EOS (as is implicitly assumed here), then in reality the d_1, d_2, \dots, d_N will not be completely independent. Thus, our way of obtaining combined results may be somewhat sub-optimal, but this just means that our conclusions about ET’s ability to reconstruct the EOS will be on the conservative side.

our analyses with r-modes included, in which case the free parameters are the ones in Eq. (15), and without r-modes, in which case the free parameters are the ones in (14), with the values for χ_{1z} and χ_{2z} set according to Eq. (18).

IV. RESULTS

We are now ready to assess the accuracy with which ET will be able to reconstruct the EOS of dense nuclear matter. However, in order to check the validity of our method, we first compare results for a simulated GW170817-like source seen in Advanced LIGO with those that were obtained in reality for GW170817. Then we turn to ET and perform an analysis on the 20 loud sources mentioned above, with or without r-modes included.

A. Analysis of a GW170817-like signal

Let us consider a signal with properties similar to that of GW170817, the binary neutron star signal discovered with LIGO and Virgo in 2017 [3]. Looking at maximum-likelihood parameter values obtained in [48], we take $(m_1, m_2) = (1.44, 1.27) M_\odot$, $\chi_{1z} = 0.022$, and $\chi_{2z} = 0.0081$. The SNR is set to 32.4, and for the Fisher matrix we take to be the one for LIGO Livingston at the time of the detection, setting $f_{\text{low}} = 23$ Hz and $f_{\text{high}} = 1625.36$ Hz. The effects of r-modes are not included, since they would have had no impact in this case. Given that we do not know what is the true equation of state, we consider the same EOS as in the rest of this paper (namely FPS), which for the given masses yields $(\Lambda_1, \Lambda_2) = (387.0, 872.2)$.

With the formalism described in the previous section, the above parameters lead to a “measurement” of $p(\rho)$. Fig. 2 shows the underlying $p(\rho)$ together with a 90% credible region. This is compared with the 90% credible region for $p(\rho)$ that was actually obtained for this event [21]. The qualitative similarity lends confidence to our methodology.

B. EOS reconstruction with Einstein Telescope

Next we turn to ET. Fig. 3 shows the EOS recovery with only the loudest source, the 5 loudest sources,

and the 20 loudest sources in our simulated catalog, with r-modes included in the way that was explained in the previous section. An improvement in measurement accuracy with increasing number of sources is clearly in evidence. We also note the narrowing of the 90% credible region near twice the nuclear saturation density, $\rho = 2\rho_{\text{sat}}$, this being the approximate average density for most of the neutron stars in our BNSs, given the EOS we picked. At $2\rho_{\text{sat}}$ and for 20

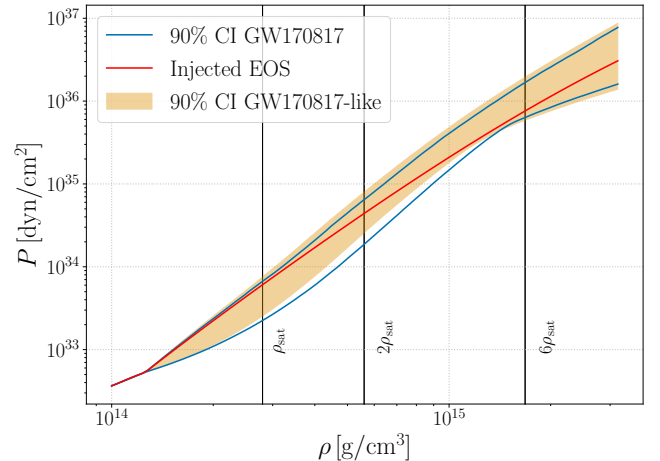


FIG. 2. Shown is pressure versus density for a GW170817-like signal whose EOS is FPS (the red curve), with a 90% credible region (orange). This is compared with the 90% credible region that was actually obtained for GW170817 (black curves) [21]. Vertical lines indicate a few multiples of the nuclear saturation density, ρ_{sat} .

sources, the width of the 90% credible interval for the pressure is 4.77×10^{33} dyn/cm², to be compared with 8.33×10^{34} dyn/cm² for our simulated GW170817 as seen by Advanced LIGO. At other densities, ET improves somewhat less on the results for GW170817; the widths $\Delta P_{90\%}(\rho)$ of the 90% credible intervals for pressure at a few different values for density are shown in Table I, for different numbers of sources in ET, with and without r-modes. Note how at $2\rho_{\text{sat}}$, a single loud source in ET improves the pressure estimation by a factor of ~ 3 over GW170817, but when combining information from 20 sources the improvement is by a factor of ~ 17 with r-modes included (and a factor of ~ 11 without r-modes). Still at $2\rho_{\text{sat}}$, the gain from r-modes reaches $\sim 50\%$.

Thus, more advanced GW observatories will dramatically improve our knowledge of the EOS, both through increased sensitivity and by seeing a larger number of

sources. The largest improvement happens near densities that actually occur in neutron stars. In Fig. 4 we show the accuracy in the measurement of pressure at

Sources	$\Delta P_{90\%}(\rho_{\text{sat}})$ [dyn/cm ²]	$\Delta P_{90\%}(2\rho_{\text{sat}})$ [dyn/cm ²]	$\Delta P_{90\%}(6\rho_{\text{sat}})$ [dyn/cm ²]
GW170817-like	7.08×10^{33}	8.33×10^{34}	2.07×10^{36}
ET, 1 source	3.47×10^{33} (3.67×10^{33})	2.62×10^{34} (3.33×10^{34})	1.50×10^{36} (1.85×10^{36})
ET, 5 sources	2.16×10^{33} (2.97×10^{33})	1.16×10^{34} (1.79×10^{34})	8.59×10^{35} (1.11×10^{36})
ET, 10 sources	8.50×10^{32} (1.71×10^{33})	5.94×10^{33} (9.37×10^{33})	5.14×10^{35} (7.33×10^{35})
ET, 20 sources	6.41×10^{32} (1.29×10^{33})	4.81×10^{33} (7.54×10^{33})	3.92×10^{35} (5.77×10^{35})

TABLE I. The widths of the 90% credible intervals for the pressure at different densities, for our GW170817-like analysis, and for ET with different numbers of sources. In the case of ET, the numbers in brackets are without r-modes.

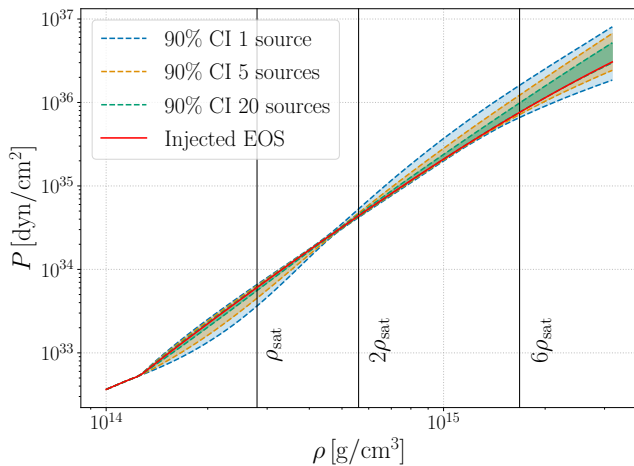


FIG. 3. 90% credible regions for pressure versus density from the loudest source, the 5 loudest sources, and the 20 loudest sources in ET, in the case where r-modes are included.

$\rho = 2\rho_{\text{sat}}$, with and without r-modes. The benefit of seeing r-modes is clearly in evidence. Note how in both cases, most of the measurement accuracy comes from combining information from the ~ 10 loudest sources.

V. SUMMARY AND CONCLUSIONS

We have investigated how well one will be able to determine the equation of state of neutron stars with Einstein Telescope, given that this observatory will detect tens of BNS inspirals per year for which the SNR will be in the hundreds. In doing so we have taken into account the effect of resonant r-modes, which provides additional information about the EOS. The latter were treated fully relativistically, both in terms of the resonance frequency and the r-mode overlap; for the former we introduced a new universal relation linking it to the neutron star tidal deformability, and for the latter we utilized the recent treatment in [27]. A reference EOS was chosen, and general EOSs were represented in terms of the so-called spectral parameterization. Simulations were performed based on the Fisher approximation of the likelihood; when identifying the tidal deformabilities Λ_i with the ones obtained from an EOS with *a priori*

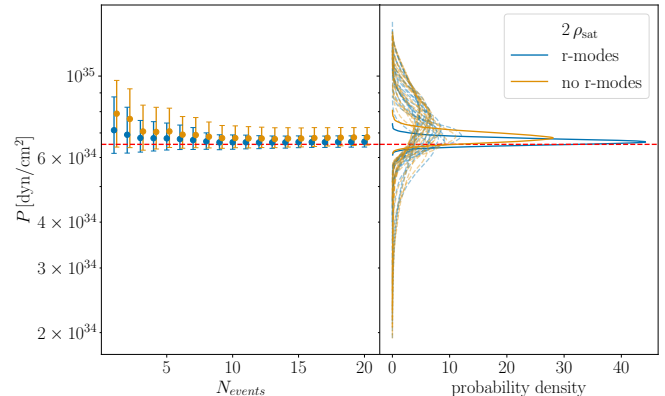


FIG. 4. Left panel: The improvement in the measurement of pressure at twice the nuclear saturation density; shown is the evolution of 90% credible intervals when going from 1 source to 20 sources, where the blue includes r-modes while the orange does not. From left to right, sources are being added in order of decreasing SNR. Right: The individual and combined probability distributions for pressure.

unknown parameters \vec{E} , sampling the likelihood leads to a PDF for \vec{E} . From this one can reconstruct the EOS in terms of pressure as a function of density. We tested our formalism on a simulated GW170817-like source, and found the accuracy of our $p(\rho)$ reconstruction to be similar to what was obtained in reality. We then turned to ET, and focused on the 20 loudest sources in a simulated “catalog” with realistic assumptions for the merger rate as a function of redshift.

The estimates arrived at in this paper are necessarily somewhat crude, due to the approximations made, and especially the limitations of the Fisher matrix formalism. We only aimed to give a rough sense of how accurately ET would be able to pin down the EOS; however, the comparison we made for GW170817 between results from our formalism and actual EOS measurements lends confidence to the reliability of our predictions.

As expected, ET will dramatically improve our knowledge of the EOS compared with what was gleaned from GW170817. In terms of $p(\rho)$, the main improvement comes at densities around twice the nuclear saturation density, since this is the typical average density of a neutron star. At that density, ET with 20 loud sources will

improve pressure measurements by a factor ~ 17 over GW170817. We found that most of the information will come from the ~ 10 loudest sources.

We also saw that the inclusion of r-modes leads to an improvement in our ability to measure the EOS, at the 50% level in terms of pressure at twice saturation density. This may seem small compared to what is suggested by [25] for a single source, but in that work, an optimistic scenario was assumed where the source had an extremely large SNR (of ~ 1500), and values for the angles ψ_1 , ψ_2 between the spins and the orbital angular momentum were chosen so as to nearly maximize the effect of r-modes on the gravitational waveform. By contrast, our sources had SNRs between 154 and 368, and randomly chosen angles ψ_i .

In this work we only considered information about the EOS coming from the inspiral part of the signal. However, ET will also have access to the merger and post-merger [49], which will lead to further improvements in the measurement of the EOS. Assessing the effect of the latter is left for future work.

ACKNOWLEDGMENTS

P.K.G., A.P., P.T.H.P., G.K., J.J., and C.V.D.B. are supported by the research programme of the Netherlands Organisation for Scientific Research (NWO). We are grateful to Tim Dietrich, Tanja Hinderer, and Jan Steinhoff for useful discussions at an early stage of the work. This research has made use of data, software and/or web tools obtained from the Gravitational Wave Open Science Center (<https://www.gwopenscience.org>), a service of LIGO Laboratory, the LIGO Scientific Collaboration and the Virgo Collaboration. LIGO is funded by the U.S. National Science Foundation. Virgo is funded by the French Centre National de Recherche Scientifique (CNRS), the Italian Istituto Nazionale della Fisica Nucleare (INFN) and the Dutch Nikhef, with contributions by Polish and Hungarian institutes.

-
- [1] J. Aasi *et al.* (LIGO Scientific), *Class. Quant. Grav.* **32**, 074001 (2015), arXiv:1411.4547 [gr-qc].
- [2] F. Acernese *et al.* (VIRGO), *Class. Quant. Grav.* **32**, 024001 (2015), arXiv:1408.3978 [gr-qc].
- [3] B. P. Abbott *et al.* (LIGO Scientific, Virgo), *Phys. Rev. Lett.* **119**, 161101 (2017), arXiv:1710.05832 [gr-qc].
- [4] B. P. Abbott *et al.* (LIGO Scientific, Virgo), (2020), arXiv:2001.01761 [astro-ph.HE].
- [5] M. Soares-Santos *et al.* (DES, Dark Energy Camera GW-EM), *Astrophys. J. Lett.* **848**, L16 (2017), arXiv:1710.05459 [astro-ph.HE].
- [6] P. S. Cowperthwaite *et al.*, *Astrophys. J. Lett.* **848**, L17 (2017), arXiv:1710.05840 [astro-ph.HE].
- [7] B. P. Abbott *et al.* (LIGO Scientific, Virgo, Fermi-GBM, INTEGRAL), *Astrophys. J. Lett.* **848**, L13 (2017), arXiv:1710.05834 [astro-ph.HE].
- [8] T. Dietrich, T. Hinderer, and A. Samajdar, *Gen. Rel. Grav.* **53**, 27 (2021), arXiv:2004.02527 [gr-qc].
- [9] M. Punturo *et al.*, *Class. Quant. Grav.* **27**, 084007 (2010).
- [10] S. Hild *et al.*, *Class. Quant. Grav.* **28**, 094013 (2011), arXiv:1012.0908 [gr-qc].
- [11] B. P. Abbott *et al.* (LIGO Scientific), *Class. Quant. Grav.* **34**, 044001 (2017), arXiv:1607.08697 [astro-ph.IM].
- [12] D. Reitze *et al.*, *Bull. Am. Astron. Soc.* **51**, 035 (2019), arXiv:1907.04833 [astro-ph.IM].
- [13] A. Samajdar, J. Janquart, C. Van Den Broeck, and T. Dietrich, *Phys. Rev. D* **104**, 044003 (2021), arXiv:2102.07544 [gr-qc].
- [14] M. Maggiore *et al.*, *JCAP* **03**, 050 (2020), arXiv:1912.02622 [astro-ph.CO].
- [15] M. Evans *et al.*, (2021), arXiv:2109.09882 [astro-ph.IM].
- [16] E. E. Flanagan and T. Hinderer, *Phys. Rev. D* **77**, 021502 (2008), arXiv:0709.1915 [astro-ph].
- [17] T. Hinderer, *Astrophys. J.* **677**, 1216 (2008), arXiv:0711.2420 [astro-ph].
- [18] W. Del Pozzo, T. G. F. Li, M. Agathos, C. Van Den Broeck, and S. Vitale, *Phys. Rev. Lett.* **111**, 071101 (2013), arXiv:1307.8338 [gr-qc].
- [19] M. Agathos, J. Meidam, W. Del Pozzo, T. G. F. Li, M. Tompitak, J. Veitch, S. Vitale, and C. Van Den Broeck, *Phys. Rev. D* **92**, 023012 (2015), arXiv:1503.05405 [gr-qc].
- [20] B. D. Lackey and L. Wade, *Phys. Rev. D* **91**, 043002 (2015), arXiv:1410.8866 [gr-qc].
- [21] B. P. Abbott *et al.* (LIGO Scientific, Virgo), *Phys. Rev. Lett.* **121**, 161101 (2018), arXiv:1805.11581 [gr-qc].
- [22] B. P. Abbott *et al.* (LIGO Scientific, Virgo), *Class. Quant. Grav.* **37**, 045006 (2020), arXiv:1908.01012 [gr-qc].
- [23] E. E. Flanagan and E. Racine, *Phys. Rev. D* **75**, 044001 (2007), arXiv:gr-qc/0601029.
- [24] E. Poisson, *Phys. Rev. D* **101**, 104028 (2020), arXiv:2003.10427 [gr-qc].
- [25] S. Ma, H. Yu, and Y. Chen, (2020), arXiv:2010.03066 [gr-qc].
- [26] A. Idrisy, B. J. Owen, and D. I. Jones, *Phys. Rev. D* **91**, 024001 (2015), arXiv:1410.7360 [gr-qc].
- [27] P. K. Gupta, J. Steinhoff, and T. Hinderer, *Phys. Rev. Res.* **3**, 013147 (2021), arXiv:2011.03508 [gr-qc].
- [28] X. Jiménez Forteza, T. Abdelsalhin, P. Pani, and L. Gualtieri, *Phys. Rev. D* **98**, 124014 (2018), arXiv:1807.08016 [gr-qc].
- [29] LIGO Scientific Collaboration, “LIGO Algorithm Library - LALSuite,” free software (GPL) (2018).
- [30] B. S. Sathyaprakash and S. V. Dhurandhar, *Phys. Rev. D* **44**, 3819 (1991).
- [31] L. Blanchet, *Living Rev. Rel.* **5**, 3 (2002), arXiv:gr-qc/0202016.
- [32] J. Vines, E. E. Flanagan, and T. Hinderer, *Phys. Rev. D* **83**, 084051 (2011), arXiv:1101.1673 [gr-qc].
- [33] L. E. Kidder, C. M. Will, and A. G. Wiseman, *Phys.*

- Rev. D **47**, R4183 (1993), arXiv:gr-qc/9211025.
- [34] L. E. Kidder, Phys. Rev. D **52**, 821 (1995), arXiv:gr-qc/9506022.
- [35] T. A. Apostolatos, C. Cutler, G. J. Sussman, and K. S. Thorne, Phys. Rev. D **49**, 6274 (1994).
- [36] W. Zhao and L. Wen, Phys. Rev. D **97**, 064031 (2018), arXiv:1710.05325 [astro-ph.CO].
- [37] P. Ade *et al.* (Planck), Astron. Astrophys. **571**, A16 (2014), arXiv:1303.5076 [astro-ph.CO].
- [38] L. Wade, J. D. E. Creighton, E. Ochsner, B. D. Lackey, B. F. Farr, T. B. Littenberg, and V. Raymond, Phys. Rev. D **89**, 103012 (2014), arXiv:1402.5156 [gr-qc].
- [39] K. Yagi and N. Yunes, Science **341**, 365 (2013), arXiv:1302.4499 [gr-qc].
- [40] P. S. Koliogiannis and C. C. Moustakidis, Astrophys. Space Sci. **364**, 52 (2019), arXiv:1806.09999 [nucl-th].
- [41] L. Lindblom, Phys. Rev. D **82**, 103011 (2010), arXiv:1009.0738 [astro-ph.HE].
- [42] F. Douchin and P. Haensel, Astron. Astrophys. **380**, 151 (2001), arXiv:astro-ph/0111092.
- [43] L. S. Finn and D. F. Chernoff, Phys. Rev. D **47**, 2198 (1993), arXiv:gr-qc/9301003.
- [44] L. S. Finn, Phys. Rev. D **46**, 5236 (1992).
- [45] B. Friedman and V. R. Pandharipande, Nucl. Phys. A **361**, 502 (1981).
- [46] D. Foreman-Mackey, D. W. Hogg, D. Lang, and J. Goodman, Publications of the Astronomical Society of the Pacific **125**, 306–312 (2013).
- [47] D. R. Lorimer, Living Rev. Rel. **11**, 8 (2008), arXiv:0811.0762 [astro-ph].
- [48] B. P. Abbott *et al.* (LIGO Scientific, Virgo), Phys. Rev. X **9**, 011001 (2019), arXiv:1805.11579 [gr-qc].
- [49] J. A. Faber and F. A. Rasio, Living Rev. Rel. **15**, 8 (2012), arXiv:1204.3858 [gr-qc].